Surface tension of bulky colloids, capillarity under gravity, and the microscopic origin of the Kardar-Parisi-Zhang equation

Luis G. MacDowell [*]

Departamento de Química-Física, Facultad de Ciencias Químicas, Universidad Complutense de Madrid, 28040 Madrid, Spain

Experimental measurements of the surface tension of colloidal interfaces have long been in conflict with computer simulations. In this Letter we show that the surface tension of colloids as measured by surface fluctuations picks up a gravity-dependent contribution which removes the discrepancy. The presence of this term puts a strong constraint on the structure of the interface which allows one to identify corrections to the fundamental equation of equilibrium capillarity and deduce bottom up the microscopic origin of a growth model with close relation to the Kardar-Parisi-Zhang equation.

A student can easily measure the surface tension of water using modest equipment such as a Nouy ring available in undergraduate laboratories. As the Nouy ring is lifted gently with a spring against surface tension *and gravity*, an equilibrium is established which reproducibly yields $\gamma = 72$ mN m^{-1} at room temperature. But is this result affected by the Earth's gravity?

Admittedly, this question looks odd at first thought. But an important consequence of renormalization theory is that interfaces must exhibit small perpendicular fluctuations of the local interfacial position which are damped by gravity [1–3]. Whereas small in amplitude, the interfacial fluctuations remain correlated over extremely large distances, corresponding to the parallel correlation length or capillary distance $\xi_\parallel^2 = \gamma/\Delta\rho\, G$ as set by the gravitational acceleration G (with $\Delta\rho$ the density difference between the bulk phases). However, this widely accepted result poses a serious problem in the limit of strong fields. Indeed, as G becomes large, it predicts a vanishing parallel correlation length, while one expects that $\xi_\parallel$ should have a lower bound that is dictated by the bulk molecular correlation length of the fluid [4]. Interestingly, the correct large and small limits of $\xi_\parallel$ may be enforced heuristically by assuming a gravity-dependent surface tension,

$$\gamma(G) = \gamma_0 + \xi^2 \Delta\rho\, G, \tag{1}$$

with γ_0 the surface tension in the absence of an external field, and ξ a measure of the bulk correlation length [5].

Unexpected as this may be, the result of Eq. (1) is difficult to rule out for a molecular fluid well away from the critical point. In view of the smallness of the bulk correlation length, which rarely is larger than a few molecular diameters, the gravity-dependent term may be estimated on the order 10^{-11} mN m^{-1} for water at room temperature, an unmeasurable correction that is a trillion times smaller than water's actual surface tension.

However, statistical mechanics has been borrowing experimental results from colloidal science for more than 30 years [6–8]. Indeed, bulky colloids of micrometer size are regularly exploited to test predictions for simple models of atomic interactions, as their size allows direct optical observation.

A paradigmatic example is the "hard-sphere" colloid, which exhibits a freezing transition and packing correlations that are in quantitative agreement with hard-sphere results obtained from computer simulations [6,7]. By use of confocal microscopy, the interface that is formed can be observed and analyzed [8–12]. Intriguingly, experimental measurements of the stiffness coefficient of those same colloidal suspensions yield widely different results in different laboratories. Some authors find results in agreement with the stiffness coefficient of the solid/liquid interface calculated in computer simulations [11,12], while others find results that differ by as much as a factor of two [9,10].

Here, we show that the surface tensions of "hard" colloid interfaces obtained in experiments show a distinct gravitational dependence (Fig. 1) that is fully consistent with Eq. (1) and allows to reconcile experimental and theoretical results. The external field dependence of the surface tension is explained bottom up in terms of an improved interface Hamiltonian which provides corrections to the fundamental equation of capillarity theory and whose growth dynamics is closely related to the Kardar-Parisi-Zhang (KPZ) model of deposition growth.

In order to illustrate the significance of Eq. (1), we first consider experimental results by Thorneywork *et al.* for two-dimensional colloidal hard spheres [13]. These authors studied the behavior of a tilted monolayer of colloids deposited on a glass surface. By selecting the appropriate surface fraction of colloids in the system, the monolayer phase separates into a liquid and a hexatic phase, with a well-defined interface. The authors studied the interfacial fluctuations by optical means, and inferred directly the stiffness coefficient from the ratio of parallel to perpendicular fluctuations as predicted by capillary wave theory in two dimensions.

———————
[*]lgmac@quim.ucm.es

FIG. 1. Stiffness coefficients of colloidal monolayers as a function of gravity. The symbols are experimental stiffness coefficients (in 10^{-16} J/m) from Ref. [13] plotted as a function of $\sin(\alpha)$, where α is the tilt angle of the inclined monolayer. The straight line is a least-squares fit under the assumption that the stiffness is a linear function of the gravity component along the inclined plane, $G \sin(\alpha)$, as dictated in Eq. (1).

Surprisingly, independent realizations of the assembled monolayers yielded significantly different stiffness coefficients. The authors attributed this to different orientations of the solid hexatic phase with respect to the interface position, and fitted their results to a model of surface anisotropy with hexagonal symmetry.

Consider instead that the colloidal hard spheres are sufficiently massive that the surface tension is affected by gravity. The tilt angle α then serves to tune the force of gravity along the inclined plane, and the component of the field in the parallel direction to the monolayer plane is given by $\Delta \rho \, G \sin(\alpha)$. Plotting the surface stiffnesses reported in Ref. [13] as a function of $\sin(\alpha)$ clearly shows an increasing trend with tilt angle, as predicted by Eq. (1) (Fig. 1). Performing a linear regression, using $G = 9.8$ ms^{-2} and a surface density difference as reported in Ref. [13], provides a good fit, with a bulk correlation length of $\xi = 10$ μm, which is a reasonable value in view of the colloid's diameter, $\sigma = 2.79$ μm. Furthermore, the zero-field stiffness, as obtained from the linear fit to Eq. (1), yields $\tilde{\gamma} d / k_B T = 0.031$, which is about one order of magnitude smaller than the related liquid/solid stiffness coefficient in three dimensions (3D), in line with expectations.

A systematic study of surface properties with gravity is not available for 3D hard-sphere colloids. However, stiffness coefficients have been measured for 3D hard-sphere colloids by Ramsteiner *et al.* [10] and van Loenen *et al.* [12]. Interestingly, Ramsteiner *et al.* performed experiments with a significant gravity effect due to a mismatch of colloid and solvent density, and found stiffness coefficients which are about twice as large as those expected in computer simulations. On the contrary, van Loenen *et al.* chose a colloidal suspension with a much closer colloid-solvent density match, and found results that are similar, albeit somewhat smaller than theoretical expectations. Indeed, the capillary wave analysis of Refs. [10,12] allows to measure the effective gravitational damping, $g'' = \Delta \rho \, G$,

TABLE I. Stiffness coefficients of hard-sphere colloids with or without a gravitational field. The second and third columns provide results for hard-sphere colloids under gravity from Ref. [10]. The fourth column displays the gravity-corrected result as described in Eq. (1). The fifth and sixth column present computer simulation results for the stiffness coefficient $\tilde{\gamma}$ and the related surface tension γ under zero gravity from Ref. [14], except for the (111) plane, from Ref. [15]. Data for the (111) plane correspond to a random stacking closed packed crystal both in experiments and simulations.

Orientation	$\beta\tilde{\gamma}\sigma^2$	$\beta g''\sigma^4$	$\beta(\tilde{\gamma} - \sigma^2\Delta\rho G)\sigma^2$	$\beta\tilde{\gamma}\sigma^2$	$\beta\gamma\sigma^2$
(100)	1.3	0.57	0.73	0.419	0.639
(100)	1.1	0.49	0.61	0.419	0.639
(110) [$\bar{1}$10]	1.0	0.37	0.63	0.769	0.616
(110) [001]	1.0	0.37	0.63	0.401	0.616
(111)	0.66	0.08	0.58	0.67	

directly from the spectrum of surface fluctuations. The results show that $\Delta \rho G$ is of the same order of magnitude as $\tilde{\gamma}$ in the experiments by Ramsteiner *et al.*, but is vanishingly small in those by van Loenen *et al.*

According to Eq. (1), the stiffness coefficients measured by Ramsteiner *et al.* should therefore be significantly affected by gravity. We can estimate the zero-field stiffness coefficients of Ref. [10], as $\tilde{\gamma}_0 = \tilde{\gamma}(G) - \xi^2 \Delta \rho G$, using $\tilde{\gamma}(G)$ and $\Delta \rho G$ obtained independently from their experiments, together with $\xi = \sigma$ as an order of magnitude estimate for the interfacial width. The results are displayed in Table I, and compared with zero gravity results obtained from computer simulations [14]. Despite some discrepancies, the table clearly shows that the gravity correction brings the experimental results in much better agreement with computer simulations. Most strikingly, the stiffness coefficient for the (100) plane, which has a large value of g'', differs by more that 260% with zero gravity results, and is brought to a 50% discrepancy upon correction from Eq. (1). On the contrary, for the randomly stacked (111) plane, which has a small value of g'', the experiments report stiffness coefficients that agree within 15 % with the zero gravity results.

The results shown here for the effect of gravity on interfacial properties are in fact a special case of a more general result regarding the dependence of stiffness coefficients on external fields, which reads [5,16,17]

$$\gamma = \gamma_0 + \xi^2 g'', \qquad (2)$$

where g'' is the second derivative of the interface potential with respect to the interface position, while ξ is an empirical measure of the interfacial width, with a similar order of magnitude as the bulk correlation length. The accuracy of this result has been tested in computer simulation studies for the special case of liquid films pinned on an inert substrate by van der Waals forces, where g'' decays as an inverse power law of the film width [5,16,18,19]. For an interface pinned by gravity, on the contrary, the interface potential is just equal to the gravitational potential energy, $g = \frac{1}{2}\Delta \rho \, Gh^2$, then $g'' = \Delta \rho \, G$ is a constant and Eq. (2) becomes equal to Eq. (1).

The result of Eq. (2) can be derived from an interface displacement model, assuming that the density of a corrugated interface $\rho(\mathbf{r})$ is a function of the perpendicular distance away

from the interface location [17]

$$\rho(\mathbf{r}) = \rho_\pi \left(\frac{z - h(\mathbf{x})}{\sqrt{1 + (\nabla h)^2}} \right), \tag{3}$$

where $\rho(\mathbf{r})$ is the fluid's density for a given realization of the fluctuations, $\rho_\pi(z)$ is the mean-field density of a flat interface, $h(\mathbf{x})$ is the interface position in the Monge representation, $\mathbf{x}$ is a point on a reference plane oriented parallel to the average interface position, and z is the perpendicular distance to that plane. This expression shows that the density profile of a corrugated interface depends not only on $h(\mathbf{x})$, but also on $\nabla h(\mathbf{x})$, which is a simple way to convey the nonlocality of corrugated interfaces on the interface position $h(\mathbf{x})$ [20].

This assumption, which has been explored in a number of studies [21,22], has been shown to be far more accurate than the standard interface displacement model $\rho(\mathbf{r}) = \rho_\pi[z - h(\mathbf{x})]$ for the description of sessile droplets barely a few molecular diameters away from the substrate [23]. In fact, using the familiar microscopic van der Waals theory of interfaces [4], Eq. (3) yields exactly the coarse-grained interface Hamiltonian model [17,21],

$$H[h] = \gamma_0 \int \sqrt{1 + (\nabla h)^2} \, d\mathbf{x}. \tag{4}$$

In the presence of an external field, the free-energy functional can become far more complex, as the intrinsic density profile $\rho_\pi(z)$ in Eq. (3) is modified by the field [24]. However, already to zero order in the density profile, there appear interesting corrections, whose significance has not been widely recognized. Indeed, assuming a local potential $V(z)$ acts on the system, one finds [18]

$$H[h] = \int d\mathbf{x} \left[\int dz \, V(z) \rho_\pi \left(\frac{z - h(\mathbf{x})}{\sqrt{1 + (\nabla h)^2}} \right) \right.$$
$$\left. + \gamma_0 \sqrt{1 + (\nabla h)^2} - \Delta p \, h(\mathbf{x}) \right], \tag{5}$$

where Δp stands for the Laplace pressure difference across the interface and we have purposely avoided explicit integration of the external field over the volume, which cannot be readily performed without additional approximations [18,25]. In the classical theory, this integral is equated to the interface potential of a flat interface evaluated at the local interface position $g(h)$. Instead, by seeking for the extremal of the free energy prior to integration of $V(z)$ over volume, we find an equilibrium condition for liquid films which goes beyond the traditional capillary approximation,

$$\frac{\tilde{\Pi}(h, h_{\mathbf{x}})}{\sqrt{1 + h_{\mathbf{x}}^2}} + \Delta p = -\frac{d}{d\mathbf{x}} \left(\frac{\gamma_0 h_{\mathbf{x}}}{\sqrt{1 + h_{\mathbf{x}}^2}} + \frac{\Delta \tilde{\gamma}(h, h_{\mathbf{x}}) h_{\mathbf{x}}}{\left(1 + h_{\mathbf{x}}^2\right)^{3/2}} \right), \tag{6}$$

where $\tilde{\Pi}(h, h_{\mathbf{x}})$ is the disjoining pressure, $\Delta \tilde{\gamma}(h, h_{\mathbf{x}})$ is the extrinsic surface tension due to the external field and $h_{\mathbf{x}}$ is used here as shorthand for ∇h. The tilde on Π and $\Delta \gamma$ denotes that these objects are actually complicated nonlocal functionals of the film profile, as conveyed by their explicit dependence on the film gradient.

In practice, for the usual case where the external field $V(z)$ varies smoothly on the scale of the interfacial width,

the h and $h_{\mathbf{x}}$ dependencies in $\tilde{\Pi}$ conveniently factor out as $\tilde{\Pi}(h, h_{\mathbf{x}}) \approx \sqrt{1 + h_{\mathbf{x}}^2} \, \Pi(h)$ with $\Pi(h)$ the disjoining pressure of a planar interface (this simplification was overlooked in Ref. [18], and lead to a linearized extremal condition that is in error). Using this result and assuming the limit of small gradients, such that $\Delta \tilde{\gamma} \to \Delta \gamma(h)$, with $\Delta \gamma(h) = \xi^2 g''(h)$, Eq. (6) now becomes a nonlinear differential equation (see Supplemental Material [26]):

$$\Pi(h) + \Delta p = -\frac{d}{d\mathbf{x}} [\gamma(h) h_{\mathbf{x}}]. \tag{7}$$

Neglecting the h dependence of $\gamma(h)$, Eq. (7) recovers the traditional Derjaguin or augmented Young-Laplace equation, which is widely used to predict the equilibrium shape and spreading dynamics of sessile droplets and capillary bridges [25,27–35]. However, Eq. (2) shows that corrections to the surface tension may become important in the neighborhood of the three-phase contact region, where $g''(h)$ becomes large.

To see this, consider the first integral of Eq. (7), which, to leading order in $g(h)/\gamma_0$, is given as (Supplemental Material [26])

$$h_{\mathbf{x}}^2 = \frac{2[g(h) - g(h_e)] + \frac{1}{2} \frac{\xi^2}{\gamma_0} \Pi^2(h)}{\gamma_0 + \xi^2 g''(h)}, \tag{8}$$

where h_e is the equilibrium film thickness of a flat film.

Away from the three-phase contact line, $\Pi^2(h)$ and $g''(h)$ decay to zero faster than does $g(h)$, and the above result recovers exactly the first integral of the Derjaguin equation [29–31]. In the neighborhood of the substrate, however, Eq. (8) provides significant corrections and dictates deviations of the film profile $h_x \approx \theta$ from the macroscopic contact angle, $\theta \approx \sqrt{-2g(h_e)/\gamma_0}$. In practice, since $\Pi^2(h)$ usually decays faster than $g''(h)$, the qualitative change may be assessed by ignoring $\Pi^2(h)$ altogether.

As an explicit example, consider a model interface potential exhibiting incomplete wetting, with an equilibrium film thickness of about two correlation lengths, and a contact angle of about $\theta = 40°$ (Supplemental Material [26]). Solving Eq. (8) for this model under the appropriate boundary conditions provides the film profile of a cylindrical liquid droplet (Fig. 2). Away from the substrate, $g(h)$ is dominated by the long-range dispersion tail, and $\Delta \gamma$ provides a small positive correction to γ_0 which has a negligible effect in the film profile. However, as the profile approaches the substrate, $\Delta \gamma$ becomes large and negative (Fig. 3 inset). As a result, the slope of $h(\mathbf{x})$ becomes larger than predicted by the Derjaguin equation, and the film profile falls sharply towards the substrate. Eventually, as h approaches the equilibrium film thickness, $\Delta \gamma$ becomes positive again and the asymptotic approach towards h_e becomes smoother than that predicted by the Derjaguin equation (Fig. 2). Therefore, the corrections due to the h dependence of the surface tension can become noticeable within a range of a few correlation lengths.

The improved functional, Eq. (5), also has interesting implications for the dynamics of interfaces. Indeed, we notice that in the small slope approximation, the nonconserved gradient-driven dynamics of the functional in Eq. (5) yields readily a deterministic nonlinear differential equation for the
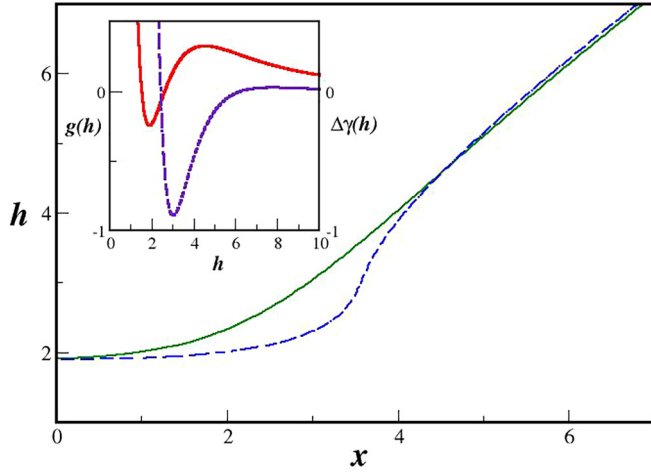
FIG. 2. Shape of liquid droplet approaching the three-phase contact line. The green (solid) line is the predicted drop profile according to the Derjaguin equation, while the blue (dashed) line corresponds to predictions from Eq. (8). The inset shows the model interface potential employed (red solid line, left axis) and $\Delta\gamma(h)$ (violet dashed line, right axis). The length scale of both figures is given in units of the correlation length, and the surface energy scale in units of γ_0.

deposition dynamics of a gas at coexistence ($\Delta p = 0$):

$$\frac{\partial h}{\partial t} = \Pi(h) + \gamma(h)\frac{d^2h}{dx^2} + \gamma'(h)\left(\frac{dh}{dx}\right)^2. \qquad (9)$$

Adding a random white-noise term, this result becomes a nonlinear stochastic growth model which may be viewed as a generalization of the celebrated Kardar-Parisi-Zhang equation (KPZ) of deposition growth [36]. Here, it is shown transparently that the nonlinear term may be obtained from an equilibrium free-energy functional, an issue that has been a matter of some debate (cf. Refs. [37,38] for a review). The bottom-up derivation makes explicit the origin of the

phenomenological coefficients, and shows that they are not fully independent.

For a thin adsorbed film above the roughening transition, the interface potential decreases with distance, and Eq. (9) yields a KPZ equation with a monotonously decaying driving and variable coefficients of the linear and quadratic terms. When the adsorbed film becomes thick enough (i.e., such as in an ordinary fluid interface), the effect of the adsorbent's external field is negligible, $g(h) \to 0$, and both the driving term and the quadratic coefficient vanish altogether, leading to a standard result of deposition growth on a fluid interface [39]. Therefore, Eq. (9) predicts for the growth of rough films a smooth crossover from a solidlike to a liquidlike deposition mechanism as the film grows. On the contrary, for a film growing below its roughening transition (as is the case of epitaxial growth), $g(h)$ is oscillatory [40]. In this case, Eq. (9) recovers the sine Gordon model of crystal growth [41,42], albeit with a quadratic correction which resembles the KPZ equation. Most interestingly, the coefficients are oscillatory, and the quadratic coefficient periodically changes sign. These features anticipate a rich behavior not predicted by the strict KPZ equation alone, and challenges the view that the constant coefficient model universally describes the long-scale behavior of growing interfaces.

In summary, we provide compelling evidence of the influence of gravity on measured surface tensions. The interfacial Hamiltonian required to explain this behavior provides corrections to the fundamental laws of capillarity theory and thin-film deposition under external fields, with potential implications in a wide range of applications.

[1] F. P. Buff, R. A. Lovett, and F. H. Stillinger, Interfacial Density Profile for Fluids in the Critical Region, Phys. Rev. Lett. **15**, 621 (1965).

[2] J. Zittartz, Microscopic approach to interfacial structure in Ising-like ferromagnets, Phys. Rev. **154**, 529 (1967).

[3] D. Jasnow, Critical phenomena at interfaces, Rep. Prog. Phys. **47**, 1059 (1984).

[4] J. Rowlinson and B. Widom, *Molecular Theory of Capillarity* (Clarendon Press, Oxford, UK, 1982).

[5] L. G. MacDowell, J. Benet, and N. A. Katcho, Capillary Fluctuations and Film-Height-Dependent Surface Tension of an Adsorbed Liquid Film, Phys. Rev. Lett. **111**, 047802 (2013).

[6] P. Pusey and W. van Mengen, Phase behavior of concentrated solutions of nearly hard colloidal spheres, Nature (London) **320**, 340 (1986).

[7] A. van Blaaderen and P. Wiltzius, Real-space structure of colloidal hard-sphere glasses, Science **270**, 1177 (1995).

[8] D. G. Aarts, M. Schmidtt, and H. N. K. Lekkerkerker, Direct observation of thermal capillary waves, Science **304**, 847 (2004).

[9] J. Hernández-Guzmán and E. R. Weeks, The equilibrium intrinsic crystal-liquid interface of colloids, Proc. Natl. Acad. Sci. USA **106**, 15198 (2009).

[10] I. B. Ramsteiner, D. A. Weitz, and F. Spaepen, Stiffness of the crystal-liquid interface in a hard-sphere colloidal system measured from capillary fluctuations, Phys. Rev. E **82**, 041603 (2010).

[11] V. D. Nguyen, Z. Hu, and P. Schall, Single crystal growth and anisotropic crystal-fluid interfacial free energy in soft colloidal systems, Phys. Rev. E **84**, 011607 (2011).

[12] S. Z. van Loenen, T. E. Kodger, E. A. Padston, S. Nawar, P. Schall, and F. Spaepen, Measurement of the stiffness of hard-sphere colloidal crystal-liquid interfaces, Phys. Rev. Mater. **3**, 085605 (2019).

[13] A. L. Thorneywork, J. L. Abbott, D. G. A. L. Aarts, and R. P. A. Dullens, Two-Dimensional Melting of Colloidal Hard Spheres, Phys. Rev. Lett. **118**, 158001 (2017).

[14] A. Härtel, M. Oettel, R. E. Rozas, S. U. Egelhaaf, J. Horbach, and H. Löwen, Tension and Stiffness of the Hard

Sphere Crystal-Fluid Interface, Phys. Rev. Lett. **108**, 226101 (2012).

[15] R. L. Davidchack, J. R. Morris, and B. B. Laird, The anisotropic hard-sphere crystal-melt interfacial free energy from fluctuations, J. Chem. Phys. **125**, 094710 (2006).

[16] L. G. MacDowell, J. Benet, N. A. Katcho, and J. M. Palanco, Disjoining pressure and the film-height-dependent surface tension of thin liquid films: New insight from capillary wave fluctuations, Adv. Colloid Interface Sci. **206**, 150 (2014).

[17] L. G. MacDowell, Capillary wave theory of adsorbed liquid films and the structure of the liquid-vapor interface, Phys. Rev. E **96**, 022801 (2017).

[18] J. Benet, J. G. Palanco, E. Sanz, and L. G. MacDowell, Disjoining pressure, healing distance, and film height dependent surface tension of thin wetting films, J. Phys. Chem. C **118**, 22079 (2014).

[19] L. G. MacDowell, P. Llombart, J. Benet, J. G. Palanco, and A. Guerrero-Martinez, Nanocapillarity and liquid bridge-mediated force between colloidal nanoparticles, ACS Omega **3**, 112 (2018).

[20] A. O. Parry, J. M. Romero-Enrique, and A. Lazarides, Nonlocality and Short-Range Wetting Phenomena, Phys. Rev. Lett. **93**, 086104 (2004).

[21] H. T. Davis, Capillary waves and the mean field theory of interfaces, J. Chem. Phys. **67**, 3636 (1977).

[22] K. R. Mecke and S. Dietrich, Effective Hamiltonian for liquid-vapor interfaces, Phys. Rev. E **59**, 6766 (1999).

[23] A. Nold, L. G. MacDowell, D. N. Sibley, B. D. Goddard, and S. Kalliadasis, The vicinity of an equilibrium three-phase contact line using density-functional theory: Density profiles normal to the fluid interface, Mol. Phys. **116**, 2239 (2018).

[24] N. R. Bernardino, A. O. Parry, C. Rascón, and J. M. Romero-Enrique, Derivation of a nonlocal interfacial model for 3D wetting in an external field, J. Phys.: Condens. Matter **21**, 465105 (2009).

[25] A. Alizadeh Pahlavan, L. Cueto-Felgueroso, A. E. Hosoi, G. H. McKinley, and R. Juanes, Thin films in partial wetting: Stability, dewetting and coarsening, J. Fluid Mech. **845**, 642 (2018).

[26] See Supplemental Material at http://link.aps.org/supplemental/10.1103/PhysRevE.108.L022801 for detailed derivation of Eq. 7, 8 and 9; as well as details of model interface potential used in Fig. 2.

[27] P. G. de Gennes, Wetting: Statics and dynamics, Rev. Mod. Phys. **57**, 827 (1985).

[28] B. Davidovitch, E. Moro, and H. A. Stone, Spreading of Viscous Fluid Drops on a Solid Substrate Assisted by Thermal Fluctuations, Phys. Rev. Lett. **95**, 244505 (2005).

[29] N. V. Churaev, Wetting Films and Wetting, Rev. Phys. Appl. (Paris) **23**, 975 (1988).

[30] P. G. de Gennes, F. Brochard-Wyart, and D. Quéré, *Capillarity and Wetting Phenomena* (Springer, New York, 2004), pp. 1–292.

[31] V. M. Starov and M. G. Velarde, Surface forces and wetting phenomena, J. Phys.: Condens. Matter **21**, 464121 (2009).

[32] H. Yin, D. N. Sibley, U. Thiele, and A. J. Archer, Films, layers, and droplets: The effect of near-wall fluid structure on spreading dynamics, Phys. Rev. E **95**, 023104 (2017).

[33] M. Durán-Olivencia, R. Gvalani, S. Kalliadasis, and G. A. Pavliotis, Instability, rupture and fluctuations in thin liquid films: Theory and computations, J. Stat. Phys. **174**, 579 (2019).

[34] Y. Zhang, J. E. Sprittles, and D. A. Lockerby, Nanoscale thin-film flows with thermal fluctuations and slip, Phys. Rev. E **102**, 053105 (2020).

[35] R. Saiseau, C. Pedersen, A. Benjana, A. Carlson, U. Delabre, T. Salez, and J.-P. Delville, Near-critical spreading of droplets, Nuovo Cimento **13**, 7442 (2022).

[36] M. Kardar, G. Parisi, and Y.-C. Zhang, Dynamic Scaling of Growing Interfaces, Phys. Rev. Lett. **56**, 889 (1986).

[37] H. S. Wio, Variational formulation for the KPZ and related kinetic equations, Int. J. Bifurcation Chaos **19**, 2813 (2009).

[38] H. Wio, J. Deza, A. Sánchez, R. García-García, R. Gallego, J. Revelli, and R. Deza, The nonequilibrium potential today: A short review, Chaos Solitons Fractals **165**, 112778 (2022).

[39] U. Thiele, Thin film evolution equations from (evaporating) dewetting liquid layers to epitaxial growth, J. Phys.: Condens. Matter **22**, 084019 (2010).

[40] A. A. Chernov and L. V. Mikheev, Wetting of Solid Surfaces by a Structured Simple Liquid: Effect of Fluctuations, Phys. Rev. Lett. **60**, 2488 (1988).

[41] Y. Saito, Statics and dynamics of the roughening transition: A self-consistent calculation, in *Ordering in Strongly Fluctuating Condensed Matter Systems*, edited by T. Riste (Plenum, New York, 1980), pp. 319–324.

[42] R. Cuerno and E. Moro, Dynamic renormalization group study of a generalized continuum model of crystalline surfaces, Phys. Rev. E **65**, 016110 (2001).